Layered Media Scattering: Fokas Integral Equations and Boundary Perturbation Methods

David P. Nicholls

Department of Mathematics, Statistics,
and Computer Science
University of Illinois at Chicago

Hamiltonian PDEs: W. Craig's 60th (Fields)

UIC

Brown University Graduation Procession (1998)

IMACS Waves Conference (Athens, GA, 1999)

Collaborators and References

Collaborator on this project:

- David Ambrose (Drexel)

Thanks to:

- NSF (DMS–1115333)
- DOE (DE–SC0001549)

References:

- Ablowitz, Fokas, & Musslimani, “On a new non-local formulation of water waves,” *JFM*, 562 (2006).
- Fokas, “A unified approach to boundary value problems,” (2008).
- Spence & Fokas, “A new transform method I & II,” *PRSL (A)*, 466 (2010).
- Deconinck & Oliveras, “The instability of periodic surface gravity waves,” *JFM*, 675 (2011).

UIC

Layered Media Scattering

- The interaction of acoustic or electromagnetic waves with periodic structures plays an important role in many scientific problems, e.g.,
  1. Seismic imaging.
  2. Underwater acoustics,
  3. Plasmonic nanostructures for biosensing,
  4. Plasmonic solar cells.

Seismic Imaging

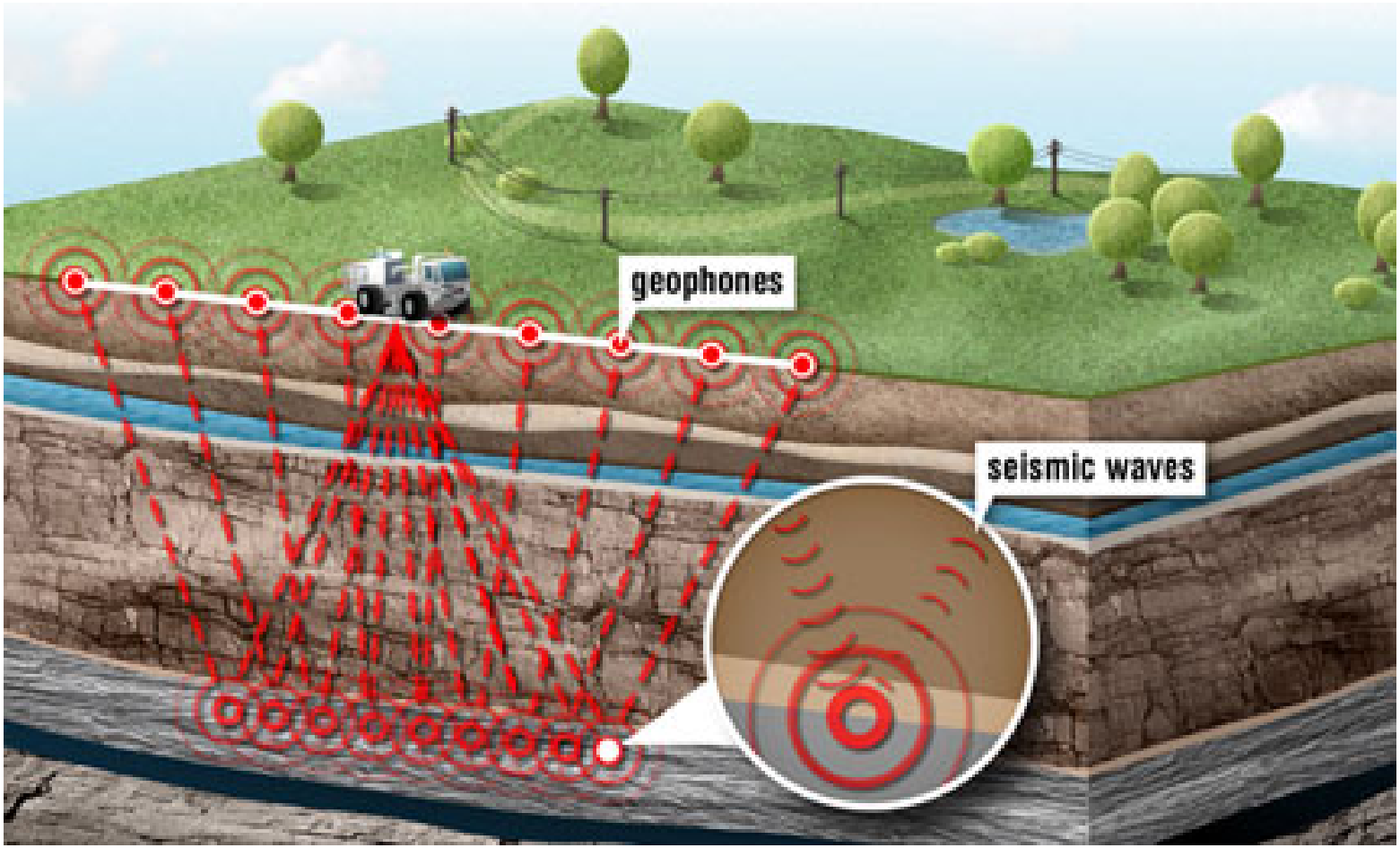

Underwater Acoustics

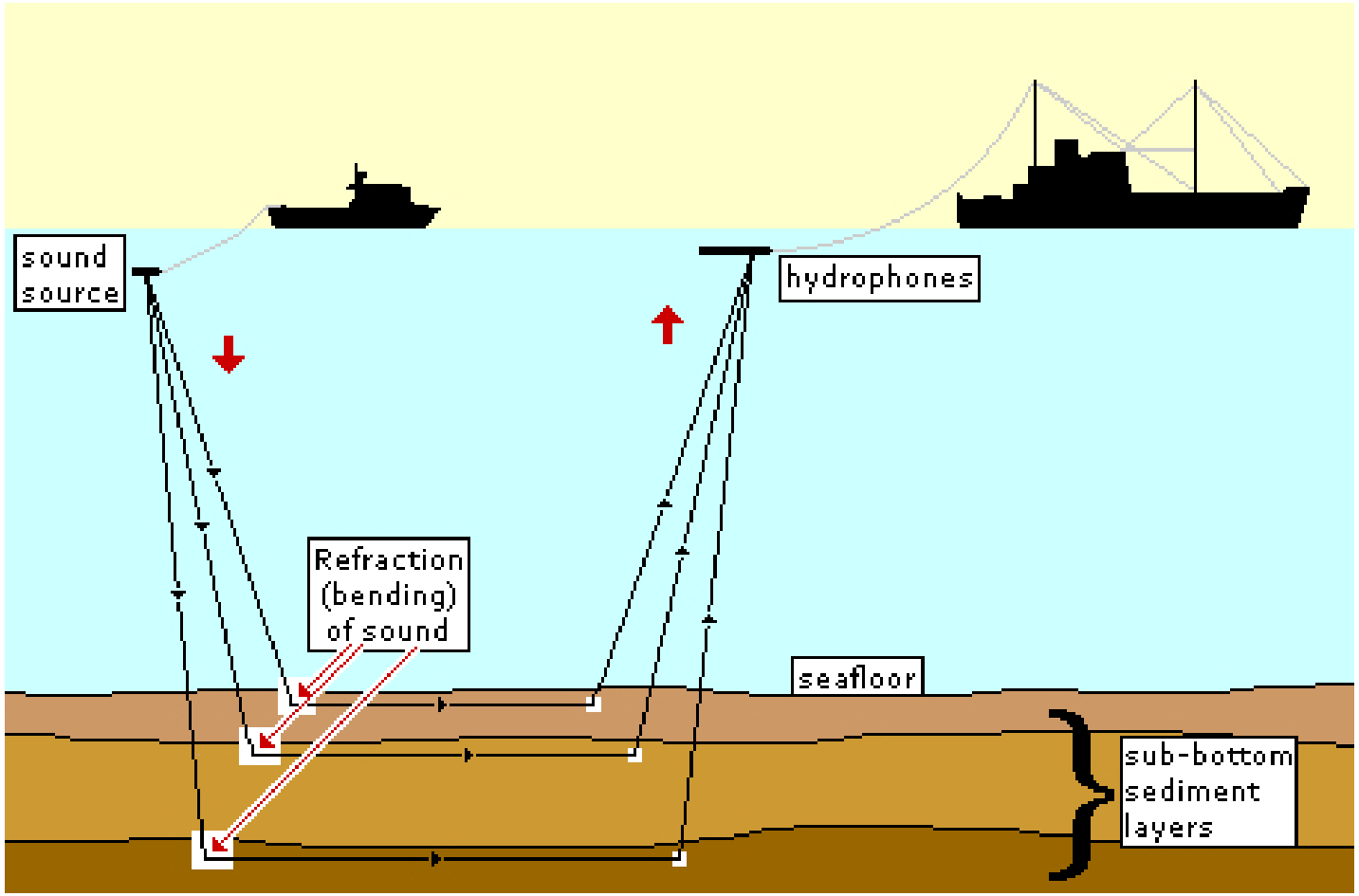

Plasmonic Nanostructures for Biosensing

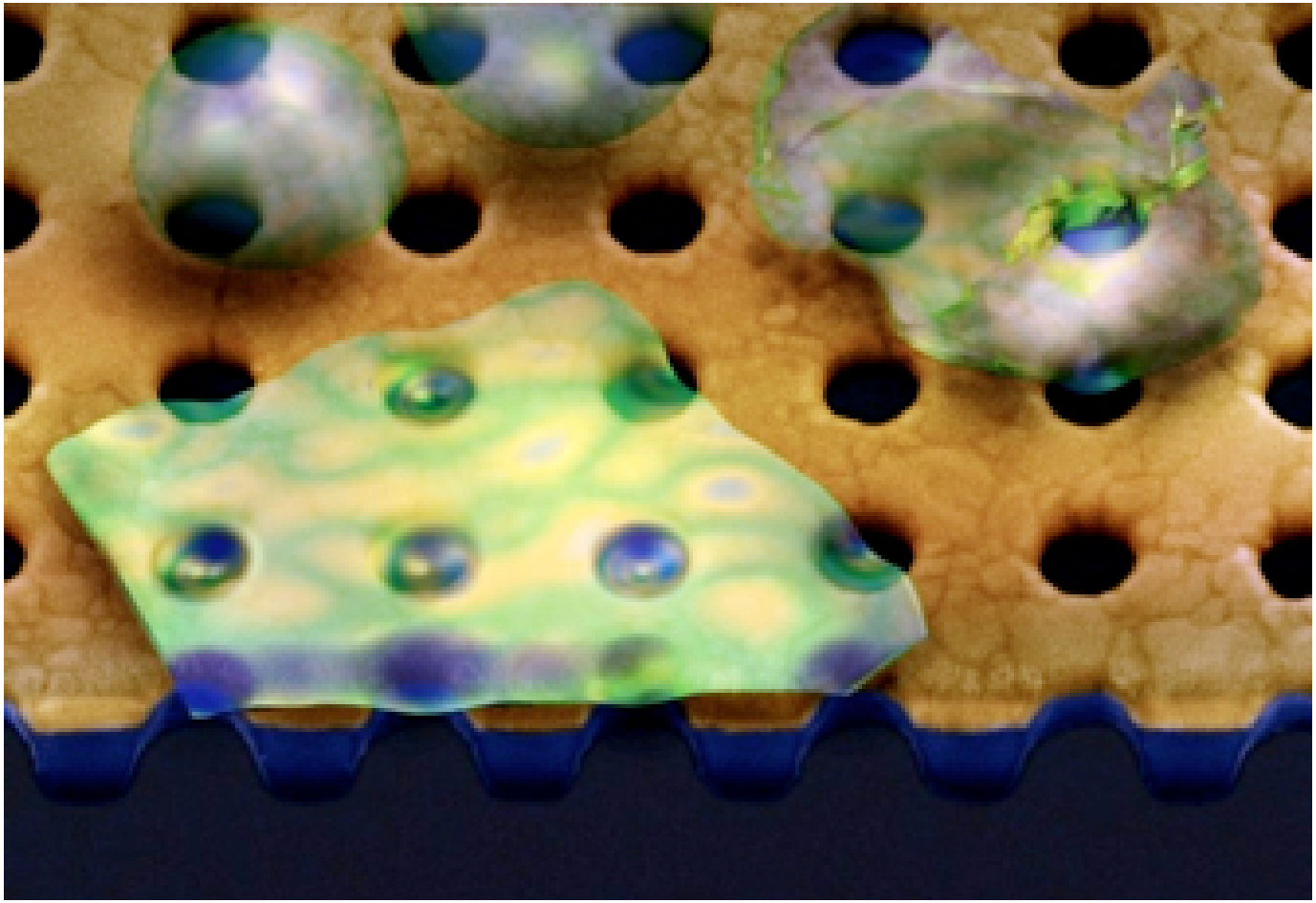

UIC

Plasmonic Solar Cells

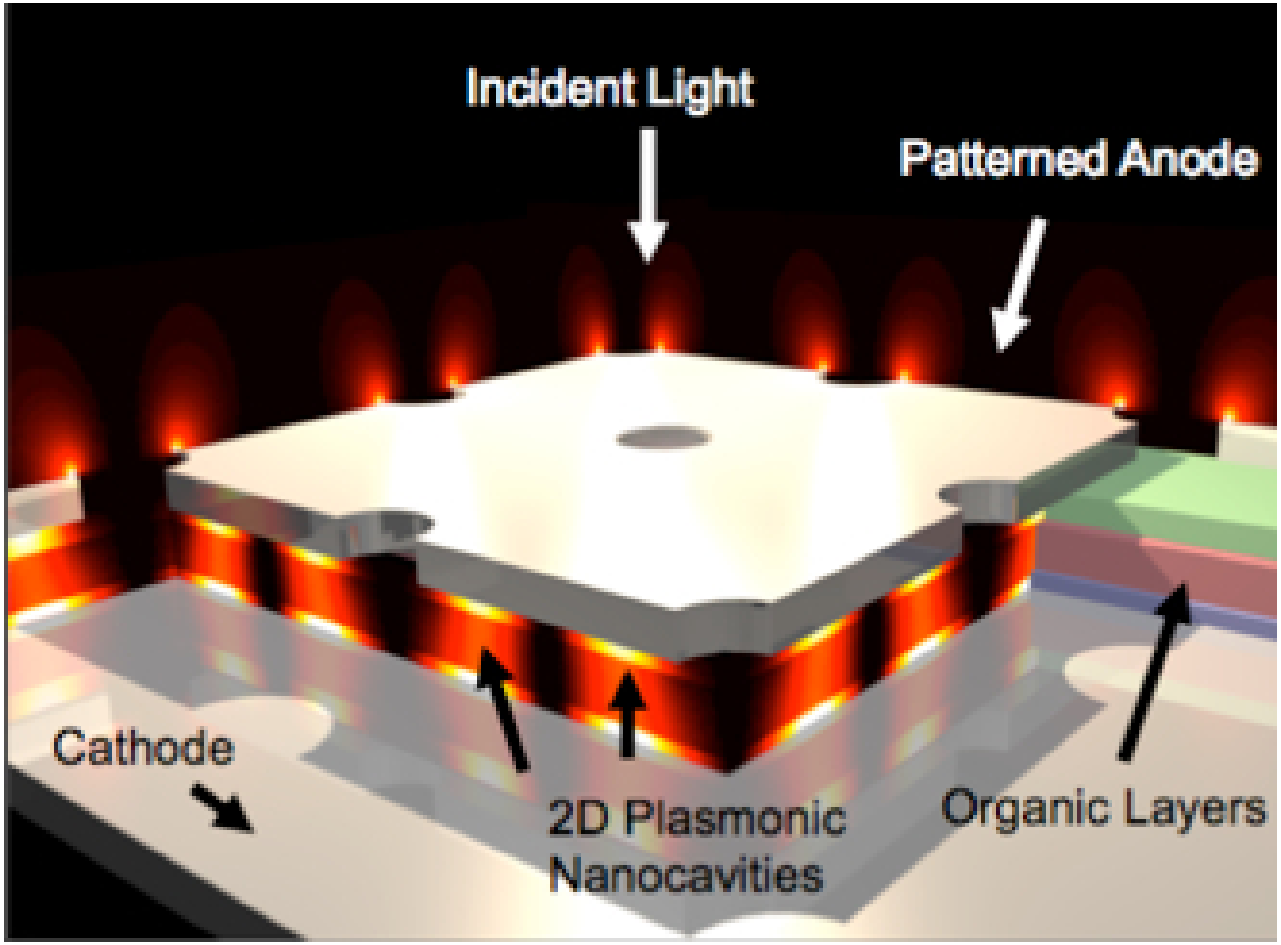

Numerical Simulation

- The ability to robustly simulate scattered fields with high accuracy is of fundamental importance.
- Here we focus upon
  1. the high–order numerical simulation
  2. of solutions of Helmholtz equations
  3. coupled across irregular (non–trivial) interfaces.
- Based upon a new surface formulation, we present a novel Integral Equation Method inspired by recent developments of Fokas and collaborators.
- Further, we extend this method using a Boundary Perturbation Method to provide an accelerated approach.

UIC

Numerical Methods: Volumetric and Surface

- Many numerical algorithms have been devised for the simulation of these problems, for instance (in the geoscience literature):
  1. Finite Differences (Pratt, 1990),
  2. Finite Elements (Zienkiewicz, 1977),
  3. Spectral Elements (Komatitsch, 2002).
- These methods suffer from the requirement that they discretize the full volume of the problem domain which results in both:
  1. A prohibitive number of degrees of freedom,
  2. The difficult question of appropriately specifying a **far–field** boundary condition explicitly.
- Surface methods are an appealing alternative and those based upon Boundary Integrals (BIM) or Boundary Elements (BEM) are very popular (e.g., Sanchez–Sesma, 1989).

UIC

Prototype Problem: Helmholtz Equation

- To illustrate the issues, consider the prototype problem: Solve the Helmholtz equation subject to Dirichlet boundary conditions

$$\Delta v + k^2 v = 0, \quad y > g(x),$$
$$v(x, g(x)) = \xi(x), \quad \mathrm{UPC}\{v\} = 0,$$

and produce the (exterior) Neumann data

$$\nu(x) = [-\partial_y u + \nabla_x g \cdot \nabla_x u]_{y=g(x)}.$$

- This mapping

$$L(g) : \xi \to \nu,$$

is the Dirichlet–Neumann Operator (DNO) which is of central importance in many fields, including water waves, acoustics, electromagnetics, and elasticity.

Maue's Method

A **standard BIM** in **acoustics**, Maue's Method, relates the **surface normal derivative**, $\nu(x)$, to (essentially) the **Dirichlet data**, ψ

$$\nu(x) - \int_{-\infty}^{\infty} K(x,x')\nu(x')\,dx' = \psi(x)$$

where

$$K(x,x') = (i\pi k/2)\rho(x,x')H_1^{(1)}(k\rho(x,x'))\zeta(x,x'),$$

and

$$\rho(x,x') = \sqrt{(x-x')^2 + (g(x)-g(x'))^2}$$

$$\zeta(x,x') = \frac{g(x) - g(x') - (\partial_x g(x))(x-x')}{(x-x')^2 + (g(x)-g(x'))^2}.$$

Maue's Method: Periodic Gratings

- If g is d–periodic we can rewrite this as

$$\nu(x) - \int_0^d K_{per}(x, x')\nu(x')\, dx' = \psi(x)$$

where

$$K_{per}(x, x') = \sum_{m=-\infty}^{\infty} K(x, x' + md).$$

- The convergence of this series is extremely slow and must be accelerated, e.g., by one of:
  1. the Spectral Representation,
  2. the Kummer Transformation,
  3. the Lattice Sum Method,
  4. the Ewald Transformation,
  5. an Integral Representation.

See Kurkcu & Reitich (*JCP*, 228 (2009)) for a nice survey.

UIC

Surface Methods

- BIM/BEM require only discretization of the layer interfaces.
- Due to the choice of the Green's function, they satisfy the far–field boundary condition exactly.
- While these methods can deliver high–accuracy simulations with greatly reduced operation counts, there are several difficulties:
  1. Devising and implementing quadrature rules which respect the singularities in the Green's function,
  2. Preconditioned iterative methods (accelerated, e.g., by Fast Multipoles) for the dense linear systems which arise.
- Later in the talk we will discuss Boundary Perturbation Methods (BPM) which which avoid these complications, e.g.,
  1. **Field Expansions**: Bruno & Reitich (1993);
  2. **Operator Expansions**: Milder (1991), Craig & Sulem (1993);
  3. **Transformed Field Expansions**: DPN & Reitich (1999).

UIC

The Method of Fokas

- We utilize Fokas' approach to discover (Fokas) Integral Equations (FIE) satisfied by the Dirichlet–Neumann Operator (DNO) and its corresponding Dirichlet data.
- These formulas do *not* involve the fundamental solution, but rather smooth, "conjugated," solutions of the periodic Helmholtz problem.
- This means simple quadrature rules (e.g., Nyström's Method) may be utilized.
- Further, periodization is unnecessary.
- Importantly, due to a clever **alternative** to the standard Green's Identity, the *derivative* of the interface never appears.
- Thus, configurations of rather low smoothness can be accommodated in comparison with standard approaches.

UIC

Key to Deriving FIE: A Divergence Lemma

Lemma (Fokas) If

$$Q^{(k)} := \partial_y \phi \left(\Delta \psi + k^2 \psi \right) + \left(\Delta \phi + k^2 \phi \right) \partial_y \psi,$$

then

$$\begin{aligned} Q^{(k)} &= \mathrm{div}_x \left[\partial_y \phi (\nabla_x \psi) + \nabla_x \phi (\partial_y \psi) \right] \\ &\quad + \partial_y \left[\partial_y \phi (\partial_y \psi) - \nabla_x \phi \cdot (\nabla_x \psi) + k^2 \phi \, \psi \right] \\ &= \mathrm{div}_x \left[F^{(x)} \right] + \partial_y \left[F^{(y)} + F^{(k)} \right], \end{aligned}$$

where

$$F^{(x)} := \partial_y \phi (\nabla_x \psi) + \nabla_x \phi (\partial_y \psi), \quad F^{(y)} := \partial_y \phi (\partial_y \psi) - \nabla_x \phi \cdot (\nabla_x \psi),$$
$$F^{(k)} := k^2 \phi \, \psi.$$

Fokas' Integral Relation

- Define the domain

$$\Omega := \left\{ \bar{\ell} + \ell(x) < y < \bar{u} + u(x) \right\},$$

- Provided that ϕ and ψ solve the Helmholtz equation we have $Q^{(k)} = 0$.
- If ϕ is α–quasiperiodic and ψ is $(-\alpha)$–quasiperiodic then the Divergence Theorem tells us

$$\begin{aligned} 0 = \int_\Omega Q^{(k)} \, \mathrm{d}V &= \int_{\partial\Omega} F \cdot \hat{n} \, \mathrm{d}S \\ &= \int_0^d \left(F^{(x)} \cdot \nabla_x \ell - F^{(y)} - F^{(k)} \right)_{y=\bar{\ell}+\ell(x)} \mathrm{d}x \\ &\quad + \int_0^d \left(F^{(x)} \cdot (-\nabla_x u) + F^{(y)} + F^{(k)} \right)_{y=\bar{u}+u(x)} \mathrm{d}x, \end{aligned}$$

since the terms $F^{(x)}$, $F^{(y)}$, and $F^{(k)}$ are *periodic*.

Surface Traces and Derivatives

If we define the surface traces

$$\xi(x) := \phi(x, \bar{\ell} + \ell(x)), \quad \zeta(x) := \phi(x, \bar{u} + u(x)),$$

then tangential derivatives are given by

$$\nabla_x \xi(x) := [\nabla_x \phi + (\nabla_x \ell)\partial_y \phi]_{y=\bar{\ell}+\ell(x)},$$
$$\nabla_x \zeta(x) := [\nabla_x \phi + (\nabla_x u)\partial_y \phi]_{y=\bar{u}+u(x)}.$$

Recall, the definitions of the DNOs give the normal derivatives

$$L(x) := [-\partial_y \phi + \nabla_x \ell \cdot \nabla_x \phi]_{y=\bar{\ell}+\ell(x)},$$
$$U(x) := [\partial_y \phi - \nabla_x u \cdot \nabla_x \phi]_{y=\bar{u}+u(x)},$$

Fokas' Relation

- In terms of these, Fokas' relation becomes

$$\int_0^d (\partial_y \psi)_{y=\bar{u}+u(x)} U \, \mathrm{d}x + \int_0^d (\partial_y \psi)_{y=\bar{\ell}+\ell(x)} L \, \mathrm{d}x$$
$$= \int_0^d (\nabla_x \psi)_{y=\bar{u}+u(x)} \cdot \nabla_x \zeta \, \mathrm{d}x - \int_0^d (\nabla_x \psi)_{y=\bar{\ell}+\ell(x)} \cdot \nabla_x \xi \, \mathrm{d}x$$
$$- \int_0^d k^2 (\psi)_{y=\bar{u}+u(x)} \zeta \, \mathrm{d}x + \int_0^d k^2 (\psi)_{y=\bar{\ell}+\ell(x)} \xi \, \mathrm{d}x.$$

- There are three terms at the top and three at the bottom.
- We will choose the test function ψ very carefully, but notice that derivatives are not applied to the boundary shapes, u and ℓ.

UIC

The Top Layer

- We give the details of the Fokas Integral Equation (FIE) relating the DNO, L, and its Dirichlet data, ξ, in the **top layer**.
- Analogous derivations can be made for the bottom and middle layers.
- Consider upward propagating, α–quasiperiodic solutions of

$$\Delta\phi + k^2\phi = 0 \qquad \bar{\ell} + \ell(x) < y < \bar{u}$$
$$\phi = \xi \qquad y = \bar{\ell} + \ell(x).$$

The Rayleigh Expansion

The Rayleigh Expansion: For $y > \bar{u}$, upward propagating, α–quasiperiodic solutions of Helmholtz equation can be written

$$\phi(x,y) = \sum_{q=-\infty}^{\infty} \hat{\zeta}_q e^{i\alpha_q \cdot x + i\beta_q (y-\bar{u})},$$

where

$$\alpha_q := \begin{pmatrix} \alpha_1 + 2\pi q_1/d_1 \\ \alpha_2 + 2\pi q_2/d_2 \end{pmatrix}, \quad \beta_q := \begin{cases} \sqrt{k^2 - |\alpha_q|^2} & q \in \mathcal{U} \\ i\sqrt{|\alpha_q|^2 - k^2} & q \notin \mathcal{U} \end{cases},$$

and the propagating modes are

$$\mathcal{U} := \left\{ q \mid |\alpha_q|^2 < k^2 \right\}.$$

A Test Function

Evaluating the Rayleigh Expansion at $y = \bar{u}$ gives $\zeta(x) = \sum_{q=-\infty}^{\infty} \hat{\zeta}_q e^{i\alpha_q \cdot x}$, so we can compute the DNO at $y = \bar{u}$:

$$U = \partial_y \phi(x, \bar{u}) = \sum_{q=-\infty}^{\infty} (i\beta_q) \hat{\zeta}_q e^{i\alpha_q \cdot x} = (i\beta_D)\zeta.$$

Consider the $(-\alpha)$–quasiperiodic "test function"

$$\psi(x, y) = e^{-i\alpha_q \cdot x + i\beta_q (y - \bar{\ell})},$$

and the upper boundary terms (1st, 3rd, 5th terms in Fokas' Relation)

$$R(x) := (\partial_y \psi)_{y=\bar{u}} U - (\nabla_x \psi)_{y=\bar{u}} \cdot \nabla_x \zeta + k^2 (\psi)_{y=\bar{u}} \zeta.$$

Using the fact that $|\alpha_p|^2 + \beta_p^2 = k^2$ we can show $\int_0^d R(x)\, dx = 0$.

UIC

Integral Equation for the Upper Layer DNO

Therefore, we can write

$$\int_0^d (\partial_y \psi)_{y=\bar{\ell}+\ell(x)} L \, \mathrm{d}x = -\int_0^d (\nabla_x \psi)_{y=\bar{\ell}+\ell(x)} \cdot \nabla_x \xi \, \mathrm{d}x + \int_0^d k^2 (\psi)_{y=\bar{\ell}+\ell(x)} \xi \, \mathrm{d}x.$$

Further, with ψ defined above

$$\int_0^d (i\beta_p) e^{i\beta_p \ell(x)} e^{-i\alpha_p x} L \, \mathrm{d}x = \int_0^d (i\alpha_p) e^{i\beta_p \ell(x)} e^{-i\alpha_p x} \cdot \nabla_x \xi \, \mathrm{d}x + \int_0^d k^2 e^{i\beta_p \ell(x)} e^{-i\alpha_p x} \xi \, \mathrm{d}x.$$

Integral Formula for Upper Layer DNO

We write this integral relation as $\hat{A}_p[L] = \hat{R}_p[\xi]$, where

$$\hat{A}_p[L] = \int_0^d (i\beta_p) e^{i\beta_p \ell} e^{-i\alpha_p \cdot x} L(x)\, dx,$$

$$\hat{R}_p[\xi] = \int_0^d e^{i\beta_p \ell} e^{-i\alpha_p \cdot x} \left\{ \frac{i\alpha_p}{i\beta_p} \cdot \nabla_x + \frac{k^2}{i\beta_p} \right\} \xi(x)\, dx.$$

We recognize the inverse Fourier transform in these formulas and solve, instead, the equation $A[L] = R[\xi]$, where

$$A = \frac{1}{|d|} \sum_{p=-\infty}^{\infty} \hat{A}_p e^{i\alpha_p \tilde{x}}, \quad R = \frac{1}{|d|} \sum_{p=-\infty}^{\infty} \hat{R}_p e^{i\alpha_p \tilde{x}}.$$

Numerical Method: We apply Nyström's Method to the equation $A[L] = R[\xi]$.

Governing Equations: Multiply–Layered Material

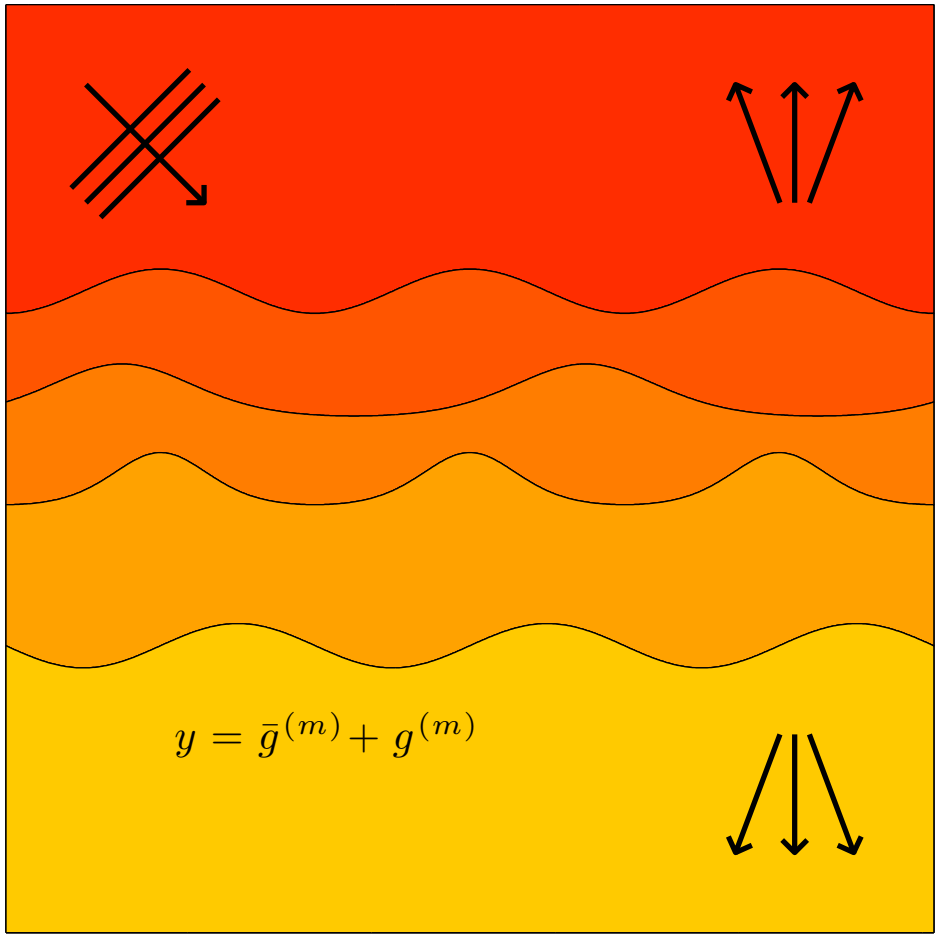

Consider a multiply–layered material with M many interfaces at

$$y = \bar{g}^{(m)} + g^{(m)}(x_1, x_2) = \bar{g}^{(m)} + g^{(m)}(x), \quad 1 \leq m \leq M,$$

separating $(M+1)$–many layers, with (upward pointing) normals

$$N^{(m)} := (-\nabla_x g^{(m)}, 1)^T.$$

Plane–Wave Incidence

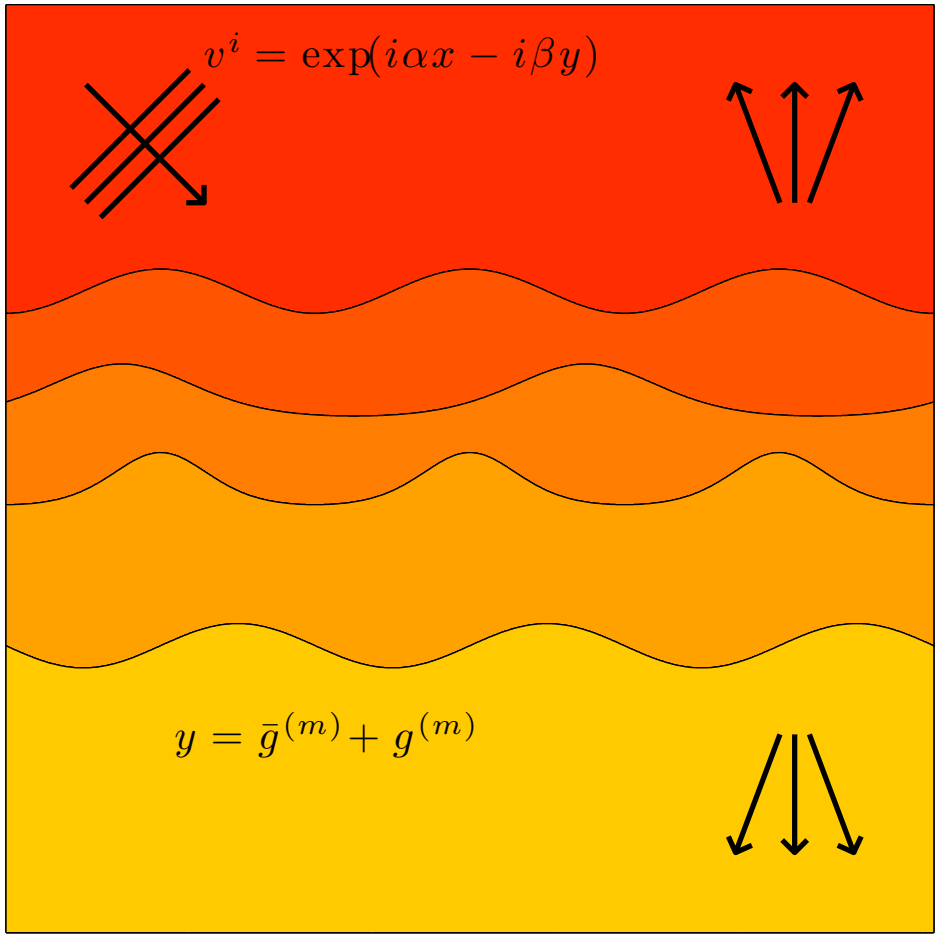

In each layer we assume a constant speed $c^{(m)}$ and that the structure is **insonified** (illuminated) from above by plane–wave acoustic incidence

$$u^i(x,y,t) = e^{-i\omega t} e^{i(\alpha \cdot x - \beta y)} =: e^{-i\omega t} v^i(x,y).$$

Time–Harmonic Scattering

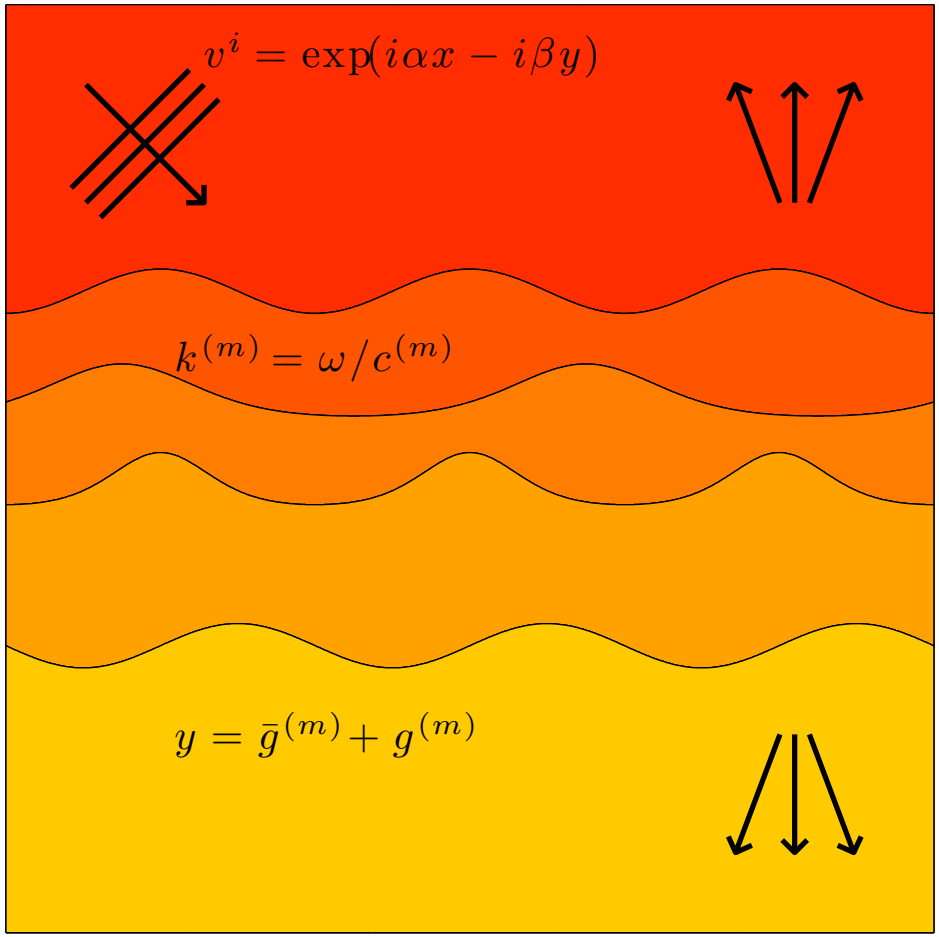

In each layer the quantity $k^{(m)} = \omega / c^{(m)}$ specifies both:

- The material properties, and
- the frequency of radiation.

These are common to both the incident and scattered acoustic fields in the structure.

Helmholtz Equations

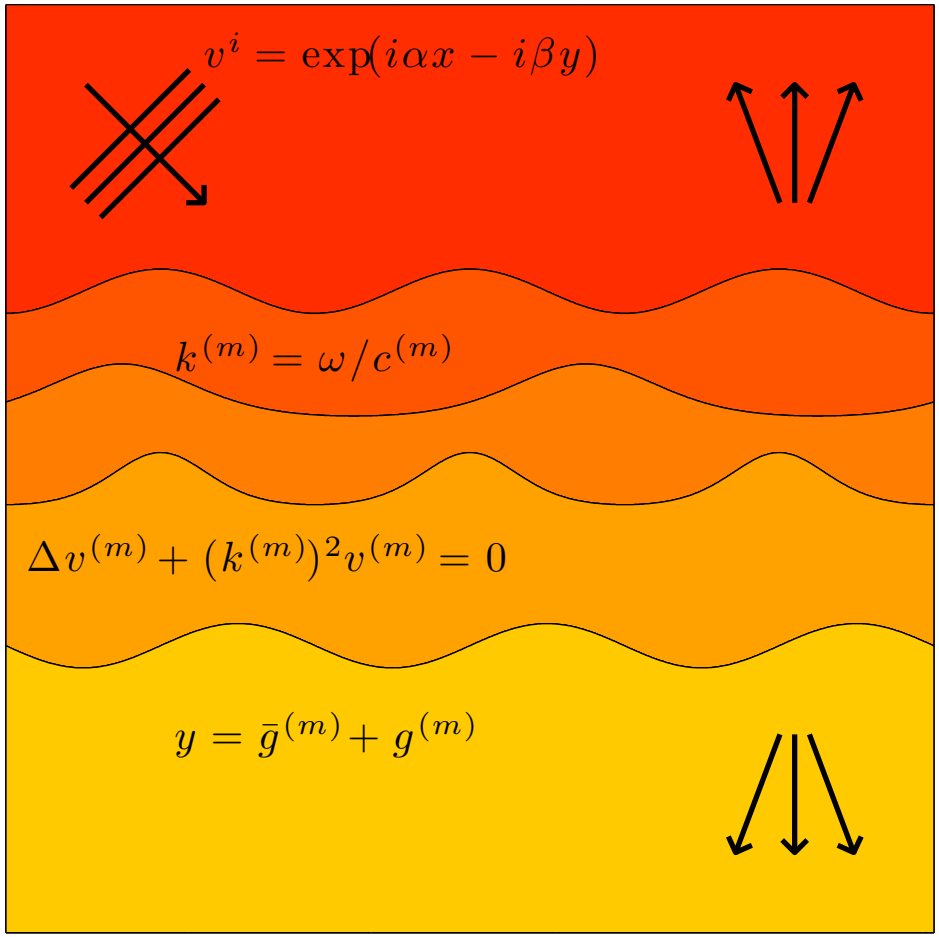

The **reduced** scattered acoustic fields satisfy Helmholtz equations in each layer:

$$\Delta v^{(m)} + (k^{(m)})^2 v^{(m)} = 0,$$
$$\bar{g}^{(m+1)} + g^{(m+1)} < y < \bar{g}^{(m)} + g^{(m)}.$$

Boundary Conditions

- It is well–known (Petit, 1980) that the problem can be restated as a time–harmonic one of time–independent **reduced** scattered fields, $v^{(m)}(x,y)$, which, in each layer, are quasiperiodic

$$v^{(m)}(x+d,y) = e^{i(\alpha\cdot d)} v^{(m)}(x,y).$$

- Boundary conditions give the coupling, for $1 \leq m \leq M$,

$$v^{(m-1)} - v^{(m)} = \zeta^{(m)} \qquad y = \bar{g}^{(m)} + g^{(m)}(x),$$

$$\partial_{N^{(m)}} \left[v^{(m-1)} - v^{(m)} \right] = \psi^{(m)}, \qquad y = \bar{g}^{(m)} + g^{(m)}(x).$$

- In the case of insonification from above

$$\zeta^{(1)} = -v^i\Big|_{y=\bar{g}^{(1)}+g^{(1)}(x)}, \quad \psi^{(1)} = -\partial_{N^{(1)}} v^i\Big|_{y=\bar{g}^{(1)}+g^{(1)}(x)},$$

$$\zeta^{(m)} \equiv \psi^{(m)} \equiv 0, \quad 2 \leq m \leq M.$$

Boundary Formulation: Dirichlet Traces

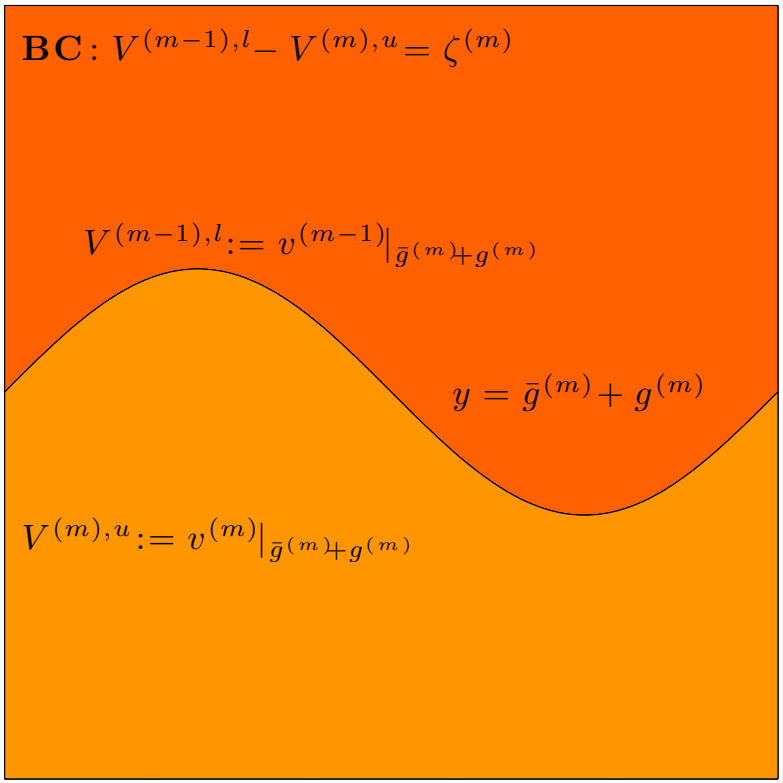

We define the Lower Dirichlet trace ($1 \leq m \leq M$):

$$V^{(m-1),l} := v^{(m-1)}\Big|_{\bar{g}^{(m)}+g^{(m)}(x)},$$

and the Upper Dirichlet trace ($1 \leq m \leq M$):

$$V^{(m),u} := v^{(m)}\Big|_{\bar{g}^{(m)}+g^{(m)}(x)}.$$

The Dirichlet boundary conditions are:

$$V^{(m-1),l} - V^{(m),u} = \zeta^{(m)}, \quad 1 \leq m \leq M.$$

Boundary Formulation: Neumann Traces

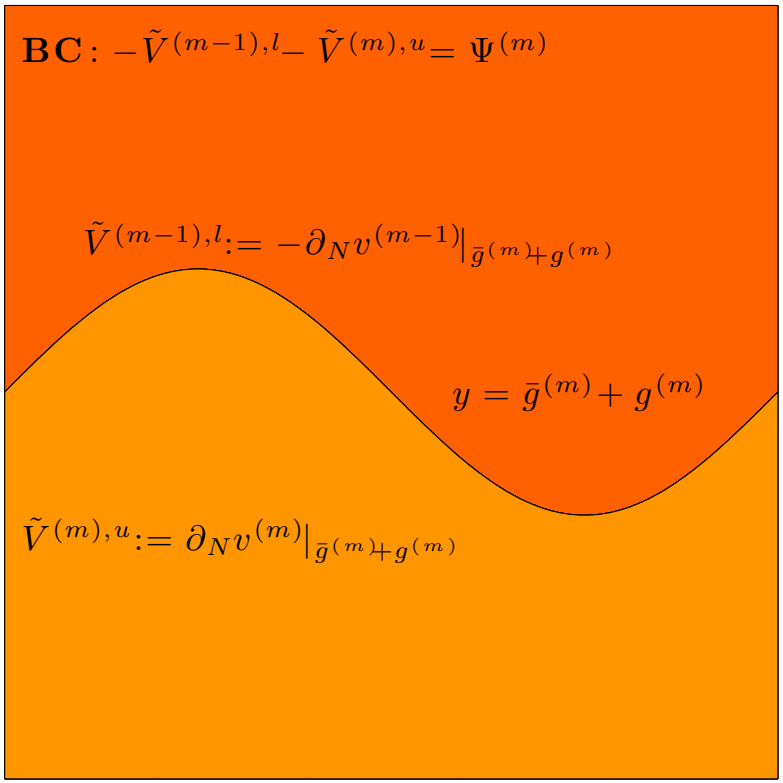

We define the Lower Neumann trace ($1 \leq m \leq M$):

$$\tilde{V}^{(m-1),l} := -\partial_{N^{(m)}} v^{(m-1)}\Big|_{y=\bar{g}^{(m)}+g^{(m)}(x)},$$

and the Upper Neumann trace ($1 \leq m \leq M$):

$$\tilde{V}^{(m),u} := \partial_{N^{(m)}} v^{(m)}\Big|_{y=\bar{g}^{(m)}+g^{(m)}(x)}.$$

The Neumann boundary conditions are:

$$-\tilde{V}^{(m-1),l} - \tilde{V}^{(m),u} = \psi^{(m)}, \quad 1 \leq m \leq M.$$

Boundary Formulation: DNOs

- We now have $(2M)$ equations for $(4M)$ unknown functions.
- This allows us to eliminate the upper traces $\{\tilde{V}^{(m),u}, V^{(m),u}\}$ in favor of the lower ones $\{\tilde{V}^{(m),l}, V^{(m),l}\}$ by

$$V^{(m),u} = V^{(m-1),l} - \zeta^{(m)} \qquad 1 \leq m \leq M$$

$$\tilde{V}^{(m),u} = -\tilde{V}^{(m-1),l} - \psi^{(m)} \qquad 1 \leq m \leq M.$$

- We can generate $(2M)$ many more equations by defining the Dirichlet–Neumann Operators (DNOs)

$$G[V^{(0),l}] := \tilde{V}^{(0),l}$$

$$H(m)[V^{(m),u}, V^{(m),l}] = \begin{pmatrix} H^{uu}(m) & H^{ul}(m) \\ H^{lu}(m) & H^{ll}(m) \end{pmatrix} \left[\begin{pmatrix} V^{(m),u} \\ V^{(m),l} \end{pmatrix} \right] := \begin{pmatrix} \tilde{V}^{(m),u} \\ \tilde{V}^{(m),l} \end{pmatrix}$$

$$J[V^{(M),u}] := \tilde{V}^{(M),u},$$

which relate the Dirichlet quantities, $\{V^{(m),u}, V^{(m),l}\}$, to the Neumann traces, $\{\tilde{V}^{(m),u}, \tilde{V}^{(m),l}\}$.

Boundary Formulation: Integral Operators

- In a moment we will derive integral operators A and R which relate the Dirichlet data, $V^{(m),I}$, to the Neumann data, $\tilde{V}^{(m),I}$.
- More specifically, for the top layer

$$A(0)\,\tilde{V}^{(0),I} - R(0)\,V^{(0),I} = 0,$$

for the middle layer

$$\begin{pmatrix} A^{uu}(m) & A^{ul}(m) \\ A^{lu}(m) & A^{ll}(m) \end{pmatrix} \begin{pmatrix} \tilde{V}^{(m),u} \\ \tilde{V}^{(m),l} \end{pmatrix} - \begin{pmatrix} R^{uu}(m) & R^{ul}(m) \\ R^{lu}(m) & R^{ll}(m) \end{pmatrix} \begin{pmatrix} V^{(m),u} \\ V^{(m),l} \end{pmatrix} = \begin{pmatrix} 0 \\ 0 \end{pmatrix} \quad 1 \leq m \leq M-1,$$

and for the bottom layer

$$A(M)\,\tilde{V}^{(M),u} - R(M)\,V^{(M),u} = 0.$$

Boundary Formulation: Linear System

Eliminating the upper traces, we write

$$A(0)\,\tilde{V}^{(0),I} - R(0)\,V^{(0),I} = 0,$$

and

$$\begin{pmatrix} A^{uu}(m) & A^{ul}(m) \\ A^{lu}(m) & A^{ll}(m) \end{pmatrix} \begin{pmatrix} -\tilde{V}^{(m-1),I} - \psi^{(m)} \\ \tilde{V}^{(m),I} \end{pmatrix}$$

$$- \begin{pmatrix} R^{uu}(m) & R^{ul}(m) \\ R^{lu}(m) & R^{ll}(m) \end{pmatrix} \begin{pmatrix} V^{(m-1),I} - \zeta^{(m)} \\ V^{(m),I} \end{pmatrix} = \begin{pmatrix} 0 \\ 0 \end{pmatrix} \quad 1 \le m \le M-1,$$

and

$$A(M)[-\tilde{V}^{(M-1),I} - \psi^{(M)}] - R(M)[V^{(M-1),I} - \zeta^{(M)}] = 0.$$

Simplifying, this can be written as

$$\mathbf{M}\mathbf{V}^{(\mathbf{I})} = \mathbf{Q}.$$

Boundary Formulation: Operator, Data, and Unknown

In this linear system, $\mathbf{MV}^{(\mathbf{I})} = \mathbf{Q}$, we have

$$\mathbf{M} := \begin{pmatrix} A(0) & -R(0) & 0 & & \cdots & 0 \\ -A^{uu}(1) & -R^{uu}(1) & A^{ul}(1) & -R^{ul}(1) & \cdots & 0 \\ -A^{lu}(1) & -R^{lu}(1) & A^{ll}(1) & -R^{ll}(1) & \cdots & 0 \\ \vdots & & & & & \vdots \\ 0 & \cdots & & 0 & -A(M) & -R(M) \end{pmatrix},$$

and

$$\mathbf{V}^{(\mathbf{I})} := \begin{pmatrix} \tilde{V}^{(0),I} \\ V^{(0),I} \\ \vdots \\ \tilde{V}^{(M-1),I} \\ V^{(M-1),I} \end{pmatrix}, \quad \mathbf{Q} := \begin{pmatrix} 0 \\ A^{uu}(1)\psi^{(1)} - R^{uu}(1)\zeta^{(1)} \\ A^{lu}(1)\psi^{(1)} - R^{lu}(1)\zeta^{(1)} \\ \vdots \\ A(M)\psi^{(M)} - R(M)\zeta^{(M)} \end{pmatrix}.$$

UIC

Numerical Results

- As we mentioned above, our numerical procedure is to apply Nyström's Method to the linear system $\mathbf{MV}^{(\mathbf{I})} = \mathbf{Q}$.
- We conduct a series of tests based upon an exact solution (possible if we ease the restriction that the data come from plane–wave incidence).
- For this we consider the functions

$$v_r^{(m)} = A^{(m)} e^{i\alpha_r \cdot x + i\beta_r^{(m)} y} + B^{(m)} e^{i\alpha_r \cdot x - i\beta_r^{(m)} y},$$

  with $A^{(M)} = B^{(0)} = 0$.
- These are outgoing, α–quasiperiodic solutions of the Helmholtz equation, however, these do not correspond to plane–wave incidence.
- We measure the maximum (relative) difference between the computed and exact values of the lower Dirichlet and Neumann traces.

Convergence Studies: Two–Dimensional Profiles

In two dimensions we consider: A smooth profile

$$f_s(x_1) = \cos(x_1),$$

a rough (C^4 but not C^5) profile

$$f_r(x_1) = (2 \times 10^{-4}) \left\{ x_1^4 (2\pi - x_1)^4 - (128\pi^8)/315 \right\},$$

and a Lipschitz profile

$$f_L(x) = \begin{cases} -(2/\pi)x + 1, & 0 \leq x \leq \pi \\ (2/\pi)x - 3, & \pi \leq x \leq 2\pi \end{cases}.$$

Remark: We point out that all three profiles have zero mean, approximate amplitude 2, and maximum slope of roughly 1.

Convergence Studies: Three–Dimensional Profiles

In three dimensions we consider: A smooth profile

$$\tilde{f}_s(x_1, x_2) = \cos(x_1 + x_2),$$

a rough (C^2 but not C^3) profile

$$\tilde{f}_r(x_1, x_2) = (2/9 \times 10^{-3}) \left\{ x_1^2 (2\pi - x_1)^2 x_2^2 (2\pi - x_2)^2 - (64\pi^8)/225 \right\},$$

and a Lipschitz profile

$$\tilde{f}_L(x_1, x_2) = \frac{1}{3} + \begin{cases} -1 + (2/\pi)x_1, & x_1 \leq x_2 \leq 2\pi - x_1 \\ 3 - (2/\pi)x_2, & x_2 > x_1, \ x_2 > 2\pi - x_1 \\ 3 - (2/\pi)x_1, & 2\pi - x_1 < x_2 < x_1 \\ -1 + (2/\pi)x_2, & x_2 < x_1, \ x_2 < 2\pi - x_1 \end{cases}.$$

Remark: We point out that all three profiles have zero mean, approximate amplitude 2, and maximum slope of roughly 1.

Smooth, Smooth Configuration (2D)

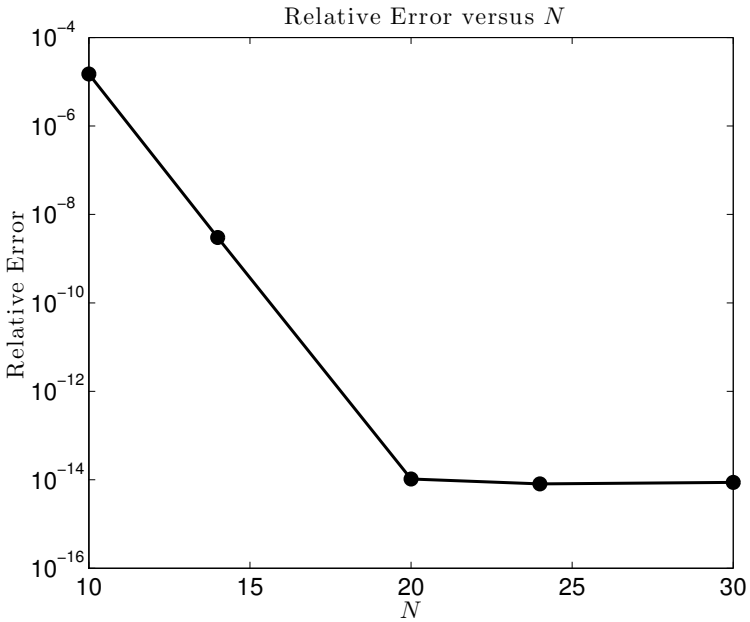

Relative error versus number of gridpoints for the **two–dimensional smooth, smooth** configuration:

$$\beta^{(0)} = 1.1, \quad \beta^{(1)} = 2.2, \quad \beta^{(2)} = 3.3,$$
$$\alpha = 0.1, \quad g^{(1)} = \varepsilon f_s, \quad g^{(2)} = \varepsilon f_s,$$
$$d = 2\pi, \quad \varepsilon = 0.01.$$

Rough, Lipschitz Configuration (2D)

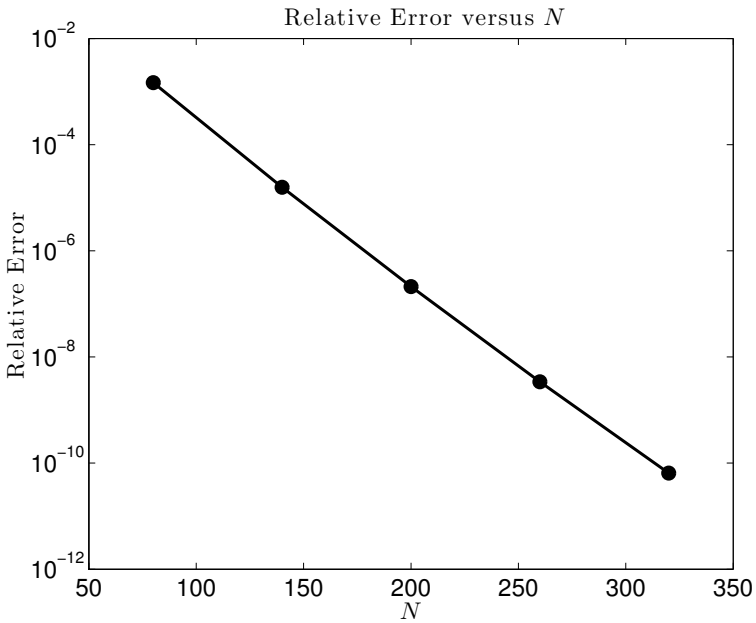

Relative error versus number of gridpoints for the **two–dimensional rough, Lipschitz** configuration:

$$\beta^{(0)} = 1.1, \quad \beta^{(1)} = 2.2, \quad \beta^{(2)} = 3.3,$$
$$\alpha = 0.1, \quad g^{(1)} = \varepsilon f_r, \quad g^{(2)} = \varepsilon f_L,$$
$$d = 2\pi, \quad \varepsilon = 0.03.$$

Smooth, Rough, Lipschitz, Rough, Smooth Configuration (2D)

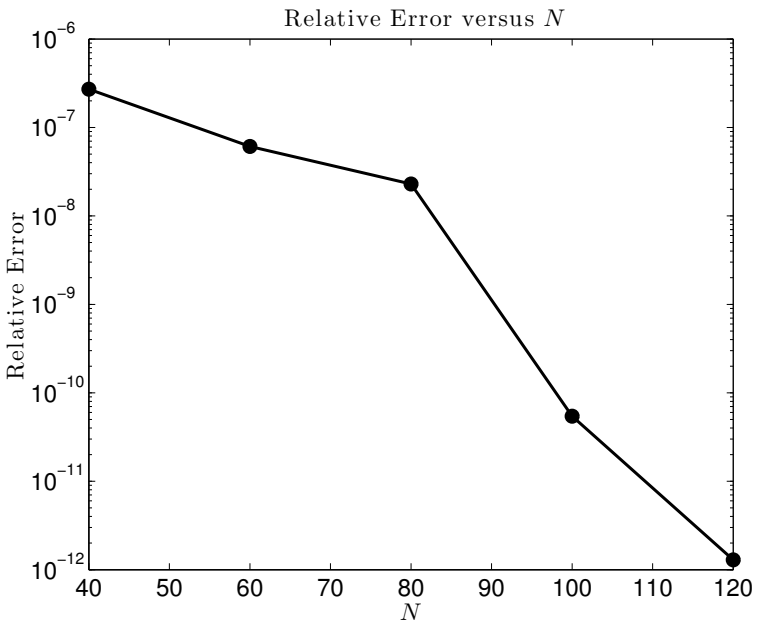

Relative error versus number of gridpoints for the **two–dimensional smooth, rough, Lipschitz, rough, smooth** configuration:

$$\beta^{(m)} = 1.1 + m, \quad 0 \leq m \leq 5,$$

$$\alpha = 0.1, \quad g^{(1)} = \varepsilon f_s, \quad g^{(2)} = \varepsilon f_r,$$

$$g^{(3)} = \varepsilon f_L, \quad g^{(4)} = \varepsilon f_r, \quad g^{(5)} = \varepsilon f_s,$$

$$d = 2\pi, \quad \varepsilon = 0.02.$$

21 Smooth Layer Configuration (2D)

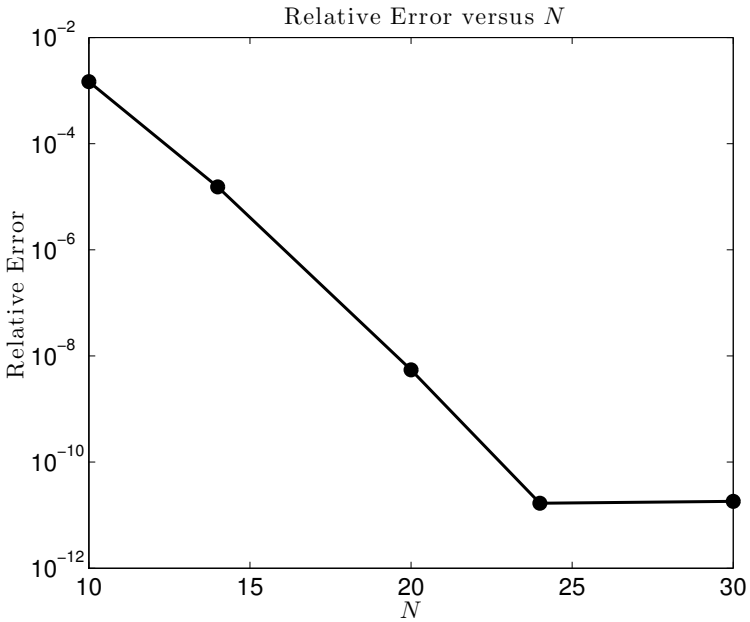

Relative error versus number of gridpoints for the **two–dimensional, 21 layer structure with smooth interfaces**:

$$\beta^{(m)} = (m+1)/10, \quad 0 \leq m \leq 20,$$

$$\alpha = 0.1, \quad g^{(m)} = \varepsilon f_s, \quad 1 \leq m \leq 20,$$

$$d = 2\pi, \quad \varepsilon = 0.02.$$

Smooth, Smooth Configuration (3D)

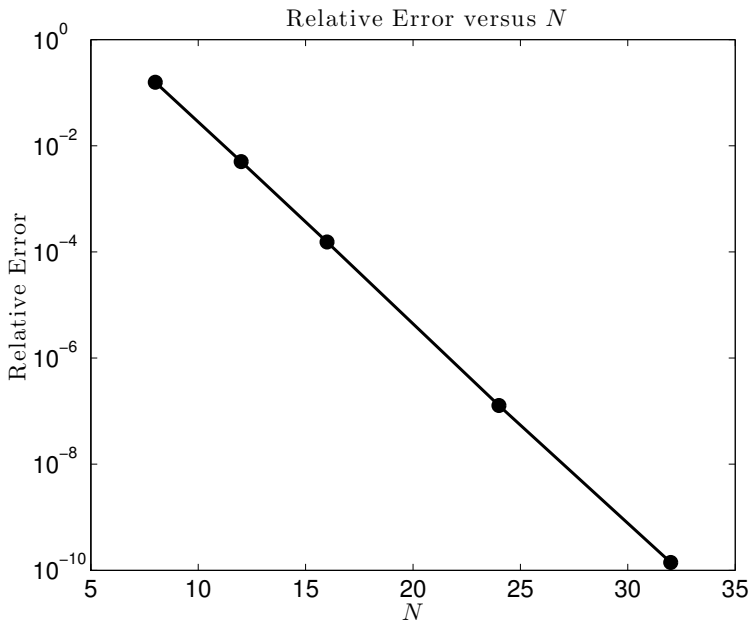

Relative error versus number of gridpoints for the **three–dimensional smooth–smooth** configuration:

$$\beta^{(0)} = 1.1, \quad \beta^{(1)} = 2.2, \quad \beta^{(2)} = 3.3,$$
$$\alpha_1 = 0.1, \quad \alpha_2 = 0.2,$$
$$g^{(1)} = \varepsilon \tilde{f}_s, \quad g^{(2)} = \varepsilon \tilde{f}_s,$$
$$d_1 = d_2 = 2\pi, \quad \varepsilon = 0.1.$$

Rough, Lipschitz Configuration (3D)

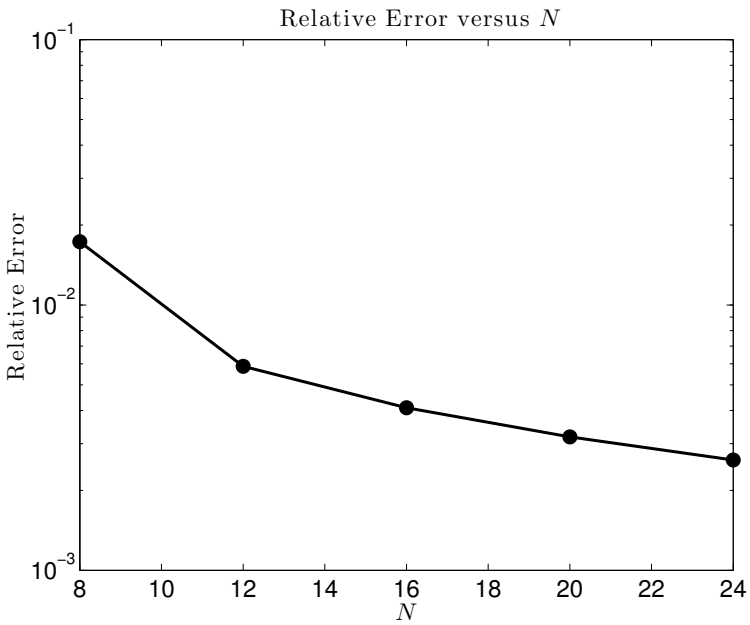

Relative error versus number of gridpoints for the **three–dimensional rough–Lipschitz** configuration:

$$\beta^{(0)} = 1.1, \quad \beta^{(1)} = 2.2, \quad \beta^{(2)} = 3.3,$$
$$\alpha_1 = 0.1, \quad \alpha_2 = 0.2,$$
$$g^{(1)} = \varepsilon \tilde{f}_r, \quad g^{(2)} = \varepsilon \tilde{f}_L,$$
$$d_1 = d_2 = 2\pi, \quad \varepsilon = 0.1.$$

A Boundary Perturbation Approach

- This FIE approach is not only flexible and simple to implement, but also highly accurate and robust.
- However, the formation and inversion of the linear operator (matrix) **M** can be quite time–consuming.
- Additionally, this operator must be inverted anew with every change in the structure (e.g., every change in the interface shapes).
- An alternative approach which can eliminate these difficulties while retaining this FIE philosophy is based upon **Boundary Perturbations**.

A Boundary Perturbation Method

- We view the boundary deformations as small deviations of flat interfaces: $g^{(m)} = \varepsilon f^{(m)}$.
- Posit (verifiable *a posteriori*) that all of the relevant integral operators depend analytically upon the perturbation parameter ε:

$$\{A, R, \mathbf{M}, \mathbf{Q}\}(\varepsilon) = \sum_{n=0}^{\infty} \{A_n, R_n, \mathbf{M}_n, \mathbf{Q}_n\} \varepsilon^n.$$

- Insert these expansions into the governing equations $\mathbf{M}\mathbf{V}^{(\mathrm{I})} = \mathbf{Q}$:

$$\left(\sum_{n=0}^{\infty} \mathbf{M}_n \varepsilon^n \right) \left(\sum_{m=0}^{\infty} \mathbf{V}^{(\mathrm{I})}{}_m \varepsilon^m \right) = \left(\sum_{n=0}^{\infty} \mathbf{Q}_n \varepsilon^n \right).$$

- At order zero we solve

$$\mathbf{M}_0 \mathbf{V}^{(\mathrm{I})}{}_0 = \mathbf{Q}_0 \quad \Longrightarrow \quad \mathbf{V}^{(\mathrm{I})}{}_0 = \mathbf{M}_0^{-1} \mathbf{Q}_0,$$

which solves the flat–interface configuration.

A Boundary Perturbation Implementation, cont.

- At orders $n > 0$ we must solve

$$\sum_{m=0}^{n} \mathbf{M}_{n-m} \mathbf{V}^{(\mathbf{I})}{}_m = \mathbf{Q}_n$$

demanding that

$$\mathbf{V}^{(\mathbf{I})}{}_n = \mathbf{M}_0^{-1} \left[\mathbf{Q}_n - \sum_{m=0}^{n-1} \mathbf{M}_{n-m} \mathbf{V}^{(\mathbf{I})}{}_m \right],$$

and we recover higher order corrections by simply inverting $\mathbf{M}_0$.

- We recall that the $\{\mathbf{M}(\varepsilon), \mathbf{Q}(\varepsilon)\}$ depend upon the $\{A(\varepsilon), R(\varepsilon)\}$ (in a somewhat complicated way) so all we need are forms for the $\{A_n, R_n\}$.

Boundary Perturbation Formula for A

- Recall the integral relation $\hat{A}_p[L] = \hat{R}_p[\xi]$, where

$$\hat{A}_p[L] = \int_0^d (i\beta_p) e^{i\beta_p \ell} e^{-i\alpha_p \cdot x} L(x)\, \mathrm{d}x,$$

and

$$A[L] = \frac{1}{|d|} \sum_{p=-\infty}^{\infty} \hat{A}_p[L] e^{i\alpha_p \tilde{x}}.$$

- It is not difficult to show that, if $\ell = \varepsilon f$,

$$\hat{A}_{n,p}[L] = \int_0^d (i\beta_p)(i\beta_p)^n \left(\frac{f^n}{n!}\right) e^{-i\alpha_p \cdot x} L(x)\, \mathrm{d}x,$$

so

$$A_n[L] = \frac{1}{|d|} \sum_{p=-\infty}^{\infty} \hat{A}_{n,p}[L] e^{i\alpha_p \tilde{x}}.$$

Numerical Results, cont.

- We return to our class of numerical simulations from earlier in the talk.
- However, for each $0 \leq n \leq N$ we apply Nyström's Method to the linear system $\mathbf{M}_n \mathbf{V}^{(\mathbf{I})}{}_n = \mathbf{Q}_n$.
- Once again we consider exact solutions, and compute maximum (relative) differences between computed and exact Dirichlet and Neumann traces.
- We consider one two–dimensional and one three–dimensional configuration from before.

UIC

(Small) Smooth, Smooth Configuration (2D)

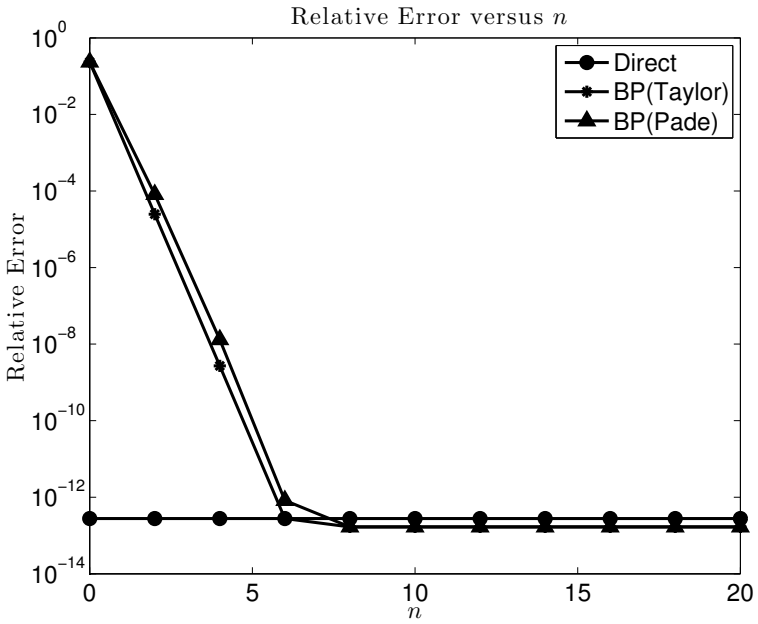

Relative error versus perturbation order for the **two–dimensional smooth, smooth** configuration:

$$\beta^{(0)} = 1.1, \quad \beta^{(1)} = 2.2, \quad \beta^{(2)} = 3.3,$$

$$\alpha = 0.1, \quad g^{(1)} = \varepsilon f_s, \quad g^{(2)} = \varepsilon f_s,$$

$$d = 2\pi, \quad \varepsilon = 0.01.$$

(Large) Smooth, Smooth Configuration (2D)

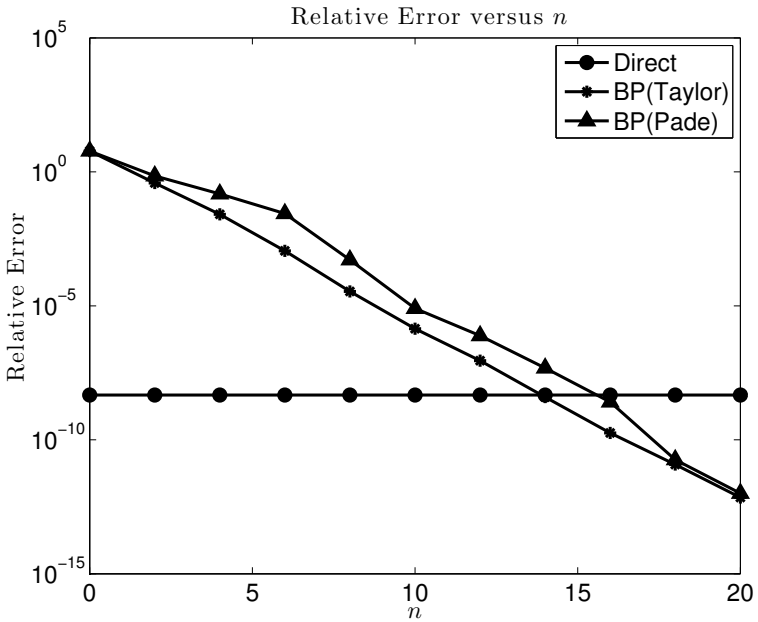

Relative error versus perturbation order for the **two–dimensional smooth, smooth** configuration:

$$\beta^{(0)} = 1.1, \quad \beta^{(1)} = 2.2, \quad \beta^{(2)} = 3.3,$$

$$\alpha = 0.1, \quad g^{(1)} = \varepsilon f_s, \quad g^{(2)} = \varepsilon f_s,$$

$$d = 2\pi, \quad \varepsilon = 0.25.$$

Two–Dimensional Conditioning and Timing

N_x	$\kappa(\mathbf{M})$	Time	$\kappa(\mathbf{M}_0)$	Time
20	331.701	1.06385	26.0527	10.6348
44	57140.3	2.94002	26.0527	21.6966
70	2.52636×10^7	8.09251	34.8825	38.1575
94	6.33777×10^9	18.8991	46.887	58.2081
120	2.0406×10^{12}	32.9924	59.8898	73.8986

UIC

Smooth, Smooth Configuration (3D)

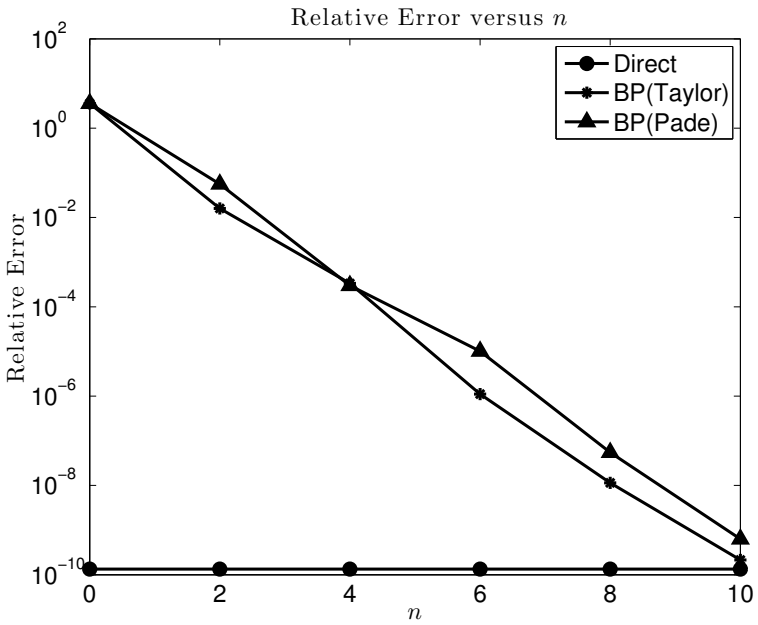

Relative error versus perturbation order for the **three–dimensional smooth–smooth** configuration:

$$\beta^{(0)} = 1.1, \quad \beta^{(1)} = 2.2, \quad \beta^{(2)} = 3.3,$$

$$\alpha_1 = 0.1, \quad \alpha_2 = 0.2,$$

$$g^{(1)} = \varepsilon \tilde{f}_s, \quad g^{(2)} = \varepsilon \tilde{f}_s,$$

$$d_1 = d_2 = 2\pi, \quad \varepsilon = 0.1.$$

Three–Dimensional Conditioning and Timing

$N_{x_1} = N_{x_2}$	$\kappa(\mathbf{M})$	Time	$\kappa(\mathbf{M}_0)$	Time
8	3174.55	8.74563	1589.91	11.2869
12	3174.55	47.6818	1589.91	25.5361
16	3174.55	206.106	1589.91	56.6273
20	3174.55	677.251	1589.91	107.622
24	3174.55	1780.91	1589.91	190.072

Summary

- The ability to robustly simulate scattered fields in periodic, layered media with high accuracy is of fundamental importance.
- Based upon a new surface formulation, we presented a novel Integral Equation Method inspired by recent developments of Fokas and collaborators.
- These formulas do *not* involve the fundamental solution, but rather smooth, "conjugated," solutions of the periodic Helmholtz problem.
- This means simple quadrature rules (e.g., Nyström's Method) may be utilized.
- Further, periodization is unnecessary.
- Importantly, due to a clever **alternative** to the standard Green's Identity, the *derivative* of the interface never appears.
- Further, we extended this method using a Boundary Perturbation Method to provide an accelerated approach.

UIC